The effects of rotation, electric field, and recycling neutrals on determining the edge pedestal density profile

W. M. Stacey[a)]
Fusion Research Center, Georgia Institute of Technology, Atlanta, Georgia 30332, USA

(Received 17 February 2010; accepted 26 April 2010; published online 19 May 2010)

The edge density profile is calculated from the continuity and momentum balance equations, using experimental electric field and rotation velocities and a calculated recycling neutral source, to evaluate the relative importance of these quantities in determining the observed structure of the edge density profile in a DIII-D [J. Luxon, Nucl. Fusion **42**, 614 (2002)] high-confinement mode discharge. © *2010 American Institute of Physics*. [doi:10.1063/1.3431092]

I. INTRODUCTION

In high-confinement H-mode plasmas, the edge density profile is observed to exhibit a "pedestal"; i.e., there is a steep gradient in the density profile starting just inside the separatrix and extending a short distance inward (the pedestal "width") until a plateau density is reached (the pedestal "height"). Understanding the structure (pedestal height and width) has long been an active area of plasma physics research (Ref. 1 reviews early work), at least in part because core transport calculations[2,3] indicate that central densities and temperatures depend on the edge pedestal values.

The limiting values of the pedestal pressure at which edge-localized mode (ELM) instabilities occur are generally understood to be determined by magnetohydrodynamic (MHD) stability limits due to ballooning modes and peeling modes, in which large bootstrap currents driven by the steep pressure gradients play a role.[4] However, the question remains of what causes these steep gradients to be formed before the MHD constraints are reached. The fact that the observed pedestal width is comparable to the mean-free-path for penetration of recycling neutrals has led to the development of models that can explain some observed edge pedestal phenomena.[5–8] Other explanations of the formation of steep gradients have been based on a sharp reduction in transport. Another observation[9] is that the experimentally observed plasma rotation and electric field require the experimentally observed ion pressure gradient in order for momentum balance to be satisfied, suggesting that understanding the causes of the rotation and electric field in the edge pedestal may be the key to understanding the edge pedestal structure.

The purpose of this paper is to document a calculation of the edge density profile in a DIII-D (Ref. 10) H-mode shot that is required by momentum and particle balance, using the measured rotation, electric field, and temperature profiles, and to compare this calculated density profile with the density profile measured by Thomson scattering. The contributions of rotation, electric field, and recycling neutrals are distinguished.

a)Electronic mail: weston.stacey@nre.gatech.edu.

II. THEORY

The theoretical formulation used in this paper is based on particle and momentum balance. A fluid model for the edge plasma was employed, with kinetic effects included in the constitutive relations for the collisional friction and viscosity. The basic equations are first written for a general ion species j in the presence of other ion species k which interact collisionally (with a sum over k implied). Subsequently the formalism is reduced to two species: a main ion species and an impurity species.

The particle continuity equation for main ion species j is

$$\nabla \cdot \Gamma_j \equiv \nabla \cdot n_j \mathbf{V}_j = S_j - \frac{\partial n_j}{\partial t}, \tag{1}$$

where $S_j = n_e(r,\theta) n_{j0}(r,\theta) \langle \sigma v \rangle_{\text{ion}} \equiv n_e(r,\theta) \nu_{\text{ion}}(r,\theta)$ is the ionization source rate of ion species j and n_{j0} is the local concentration of neutrals of species j. These neutrals include neutral atom recycling from the plasma chamber wall and those deposited by neutral beam injection (for which the ionization rate needs to be expanded to include also the charge-exchange rate). The source for impurity ions is more complex.

The time-dependent momentum balance equation for ion species j is

$$\begin{aligned} \nabla \cdot (n_j m_j \mathbf{V}_j \mathbf{V}_j) + \nabla p_j + \nabla \cdot \boldsymbol{\pi}_j \\ = n_j e_j (\mathbf{V}_j \times \boldsymbol{B}) + n_j e_j \boldsymbol{E} + \boldsymbol{F}_j + \boldsymbol{M}_j \\ - n_j m_j \nu^j_{\text{elcx}j} \mathbf{V}_j - \frac{\partial (n_j m_j \mathbf{V}_j)}{\partial t}, \end{aligned} \tag{2}$$

where p_j is the pressure, $\boldsymbol{\pi}_j$ represents the viscous momentum flux, $\mathbf{E}$ represents the electric field, $\mathbf{F}_j = -n_j m_j \nu_{jk} (\mathbf{V}_j - \mathbf{V}_k)$ represents the interspecies collisional friction, $\mathbf{M}_j$ represents the external momentum input rate (e.g., due to neutral beams), the next-to-last term represents the momentum loss rate due to elastic scattering and charge exchange with neutrals of all ion species $k[\nu_{\text{elcx}j} = \Sigma_k n^c_{k0} (\langle \sigma v \rangle_{\text{el}} + \langle \sigma v \rangle_{\text{cx}})_{jk}]$, and as usual $(n_j, m_j, e_j, \mathbf{V}_j)$ denote particle density, mass, charge, and velocity of species j.

The toroidal and radial components of the momentum balance equation for ion species j can be written as

$$n_j m_j[(\nu_{jk}+\nu_{dj})V_{\phi j}-\nu_{jk}V_{\phi k}]=n_j e_j E_\phi^A+n_j e_j B_\theta V_{rj}+M_{\phi j} \tag{3}$$

and

$$V_{\phi j}=\frac{1}{B_\theta}\left(E_r+V_{\theta j}B_\phi-\frac{1}{n_j e_j}\frac{\partial p_j}{\partial r}\right), \tag{4}$$

where ν_{dj} is the toroidal angular momentum transfer frequency due to viscosity, inertial forces, atomic physics reactions with neutral atoms, and other "anomalous" processes (justification for representing these processes in this form is discussed in Ref. 11), E_ϕ^A is the induced electromagnetic field, M_ϕ is the rate of toroidal momentum deposition due to neutral beams or other sources, and the other symbols have their usual meaning. In general, the subscript k represents a sum over other ion species, but in this paper we consider only a single other species (i.e., an "ion-impurity" deuterium plasma with an "average charge state" carbon impurity).

Using Eq. (4) to eliminate the toroidal velocities for both species, Eq. (3) may be rewritten

$$\begin{aligned}V_{rj}&=-\frac{m_j(\nu_{jk}+\nu_{dj})T_j}{(e_jB_\theta)^2}\left[\left(\frac{1}{p_j}\frac{\partial p_j}{\partial r}\right)-\frac{e_j}{e_k}\frac{\nu_{jk}}{(\nu_{jk}+\nu_{dj})}\left(\frac{1}{p_k}\frac{\partial p_k}{\partial r}\right)\right]\\&\quad+V_{rj}^{\text{pinch}}\\&\simeq-\frac{m_j(\nu_{jk}+\nu_{dj})T_j}{(e_jB_\theta)^2}\left(\frac{1}{p_j}\frac{\partial p_j}{\partial r}\right)+V_{rj}^{\text{pinch}}\end{aligned} \tag{5}$$

for the main ions, where

$$V_{rj}^{\text{pinch}}=\frac{1}{e_jB_\theta}\left[-\left(e_jE_\phi^A+\frac{M_{\phi j}}{n_j}\right)+\frac{m_j\nu_{dj}}{B_\theta}(E_r+V_{\theta j}B_\phi)+\frac{m_j\nu_{jk}B_\phi}{B_\theta}(V_{\theta j}-V_{\theta k})\right]. \tag{6a}$$

Using the above momentum balance relations to eliminate only the main toroidal velocity leads to a similar result, but with

$$V_{rj}^{\text{pinch}}=\frac{[-M_{\phi j}-n_je_jE_\phi^A+n_jm_j(\nu_{jk}+\nu_{dj})(f_p^{-1}V_{\theta j}+E_r/B_\theta)-n_jm_j\nu_{jk}V_{\phi k}]}{n_je_jB_\theta}, \tag{6b}$$

where $f_p=B_\theta/B_\phi$.

Defining an effective main ion diffusion coefficient for convenience of notation

$$D_j=\frac{m_jT_j\nu_{jk}}{(e_jB_\theta)^2}\left(1+\frac{\nu_{dj}}{\nu_{jk}}-\frac{Z_j}{Z_k}\right). \tag{7}$$

Equation (5) can be rearranged to define an algorithm,

$$\frac{-1}{p_i}\frac{\partial p_j}{\partial r}=\frac{V_{rj}-V_{rj}^{\text{pinch}}}{D_j}, \tag{8}$$

that can be integrated to solve for the ion density ($n_j=p_j/kT_j$) profile in the edge pedestal in terms of the measured rotation velocities and electric field, which enter V_{rj}^{pinch}, and the recycling neutral source which is used in the continuity Eq. (1) to solve for the radial ion velocity V_{rj}.

III. EXPERIMENTAL DATA

An ELMing H-mode, lower single null DIII-D discharge (No. 98889: I=1.2 MA, B=2.0 T, P_{nbi}=3.1 MW, $n=4\times10^{19}/\text{m}^3$) that is being analyzed in some detail for the H-mode edge pedestal benchmarking activity[12] was selected. Data were averaged over the same subinterval (80%–99%) between ELMs for several successive ELMs in order to minimize the effect of random errors, and the data set is identified as "4500." Fits of the measured electron density and electron and ion temperature profiles are shown in Fig. 1. Fits of the measured carbon poloidal and toroidal rotation velocities are shown in Fig. 2. The measurements and data analysis are discussed in detail for the density and temperatures in Ref. 13 and for the rotation velocities in Ref. 14.

Also shown in Fig. 2 are calculated deuterium rotation velocities. The deuterium toroidal velocity was calculated by a perturbation method using the measured carbon toroidal velocity to infer an experimental angular momentum transfer rate,[14] then solving the deuterium toroidal momentum balance equation for the difference in the carbon and deuterium toroidal velocities, using this inferred momentum transfer rate (to represent viscous and atomic physics momentum losses) and the measured carbon toroidal rotation.

The measured density and temperature profiles of Fig. 1 were used to evaluate these equations. Neutral atom recy-

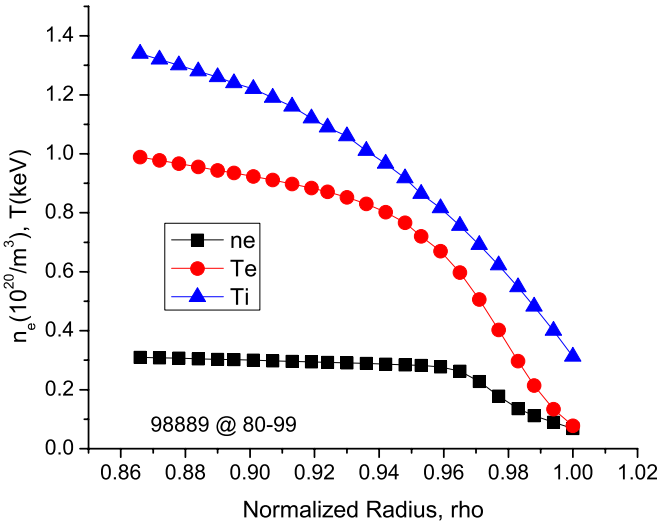

FIG. 1. (Color online) Experimental density and temperatures.

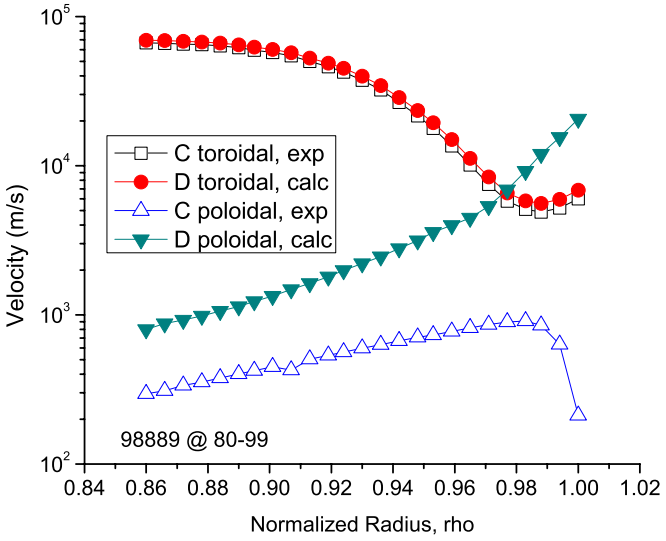

FIG. 2. (Color online) Experimental and calculated rotation velocities.

cling was calculated using a two-dimensional (2D) model of the edge region and divertor.

We use the measured carbon toroidal rotation velocity as input in solving the toroidal momentum balance equations backward to infer the local momentum transport frequencies from the toroidal angular momentum equation. Equation (3) for each species can readily be rearranged to yield (for the two-ion-species model) a requirement on the composite angular momentum transport frequency for all mechanisms (classical and anomalous viscosity, inertial, atomic physics, etc.) that must be satisfied in order to produce the measured rotation velocities

$$\nu_{dj} = \nu_{jk}\left[\frac{n_j e_j E_\phi^A + e_j B_\theta \Gamma_{rj} + M_{\phi j}}{n_j m_j \nu_{jk} V_{\phi j}} - \left(1 - \frac{V_{\phi k}}{V_{\phi j}}\right)\right] \tag{9}$$

(and a similar expression with the j and k subscripts interchanged). All quantities on the right except the rotation velocities readily can be determined from measurements and solving the continuity equation. Thus, if the toroidal rotation velocities for both ion species are also measured, the momentum transfer frequencies for both species can be determined from Eq. (9) (plus the same equation with j and k interchanged).

An immediate problem is encountered because the deuterium rotation velocities are not measured. To get around this problem, we use a perturbation analysis of the above toroidal momentum balance equations for a two-species (deuterium j, carbon impurity k) plasma to first obtain an estimate of the difference in the deuterium and carbon toroidal velocities. This difference can be added to the measured carbon velocity to obtain a deuterium toroidal velocity. The measured carbon velocity and the so-constructed deuterium velocity can then be used to solve the toroidal momentum balance equations "backward" for the experimental angular momentum transfer frequencies (arising from all processes including anomalous ones) that are required in order for the toroidal momentum balance equations to yield the two "experimental" toroidal velocities.

First, the toroidal momentum balance Eq. (3) for the two species are added to eliminate the friction terms and used to define an effective momentum transfer frequency

$$\nu_d^{\text{eff}} \equiv \frac{n_j m_j \nu_{dj} + n_k m_k \nu_{dk}}{n_j m_j + n_k m_k} = \frac{(n_j e_j E_\phi^A + e_j B_\theta \Gamma_{rj} + M_{\phi j}) + (n_k e_k E_\phi^A + e_k B_\theta \Gamma_{rk} + M_{\phi k}) - \{n_j m_j \nu_{dj}(V_{\phi j} - V_{\phi k})\}}{(n_j m_j + n_k m_k) V_{\phi k}}. \tag{10}$$

The { } term involving the difference in toroidal velocities is set to zero to obtain a zeroth order approximation of the effective momentum transport frequency ν_d^0,

$$\nu_d^0 = \frac{(n_j e_j E_\phi^A + e_j B_\theta \Gamma_{rj} + M_{\phi j}) + (n_k e_k E_\phi^A + e_k B_\theta \Gamma_{rk} + M_{\phi k})}{(n_j m_j + n_k m_k) V_{\phi k}^{\text{exp}}}. \tag{11}$$

In the limit of vanishing impurity concentration, Eq. (11) would approach the deuterium momentum transfer frequency, which motivates its use as the zero order approximation for the deuterium momentum transfer frequency. Using this expression, along with the measured carbon toroidal velocity $V_{\phi k}^{\text{exp}}$ in Eq. (3) for the deuterium, j species yields a zeroth order approximation for the deuterium-carbon velocity difference

$$(V_{\phi j} - V_{\phi k})_0 = \frac{(n_j e_j E_\phi^A + e_j B_\theta \Gamma_{rj} + M_{\phi j}) - n_j m_j \nu_d^0 V_{\phi k}^{\text{exp}}}{n_j m_j (\nu_{jk} + \nu_d^0)}, \tag{12}$$

which in turn is used in Eq. (3) for the carbon impurity k species to solve for the carbon momentum transport frequency

$$\nu_{dk} = \frac{(n_k e_k E_\phi^A + e_k B_\theta \Gamma_{rk} + M_{\phi k}) + n_k m_k \nu_{kj}(V_{\phi j} - V_{\phi k})_0}{n_k m_k V_{\phi k}^{\text{exp}}}. \tag{13}$$

The deuterium momentum transfer frequency is then calculated from the definition of Eq. (11) using $\nu_d^{\text{eff}} \approx \nu_d^0$, which yields $\nu_{dj} \approx \nu_d^0$.

The experimentally inferred deuterium and carbon momentum transfer frequencies are shown in Fig. 3. Also shown is the deuterium-carbon collision frequency ν_{jk}. The calculated $V_{\phi j}$ for deuterium is very similar to the carbon toroidal rotation velocity, as shown in Fig. 2. Note that the inferred momentum transfer rate due to viscosity, atomic physics, and

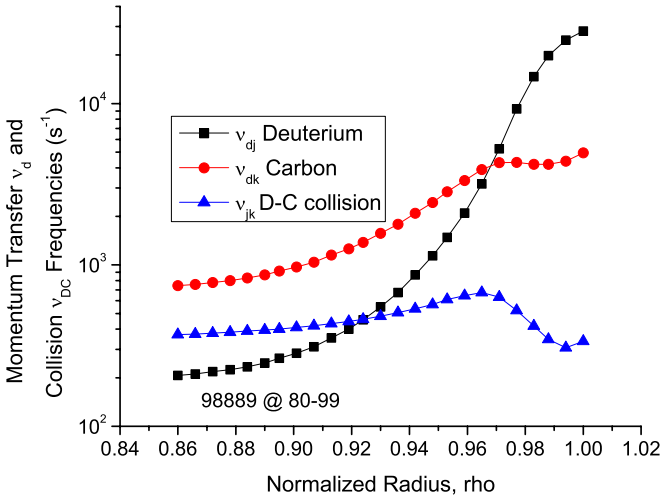

FIG. 3. (Color online) Angular momentum transfer and collision frequencies.

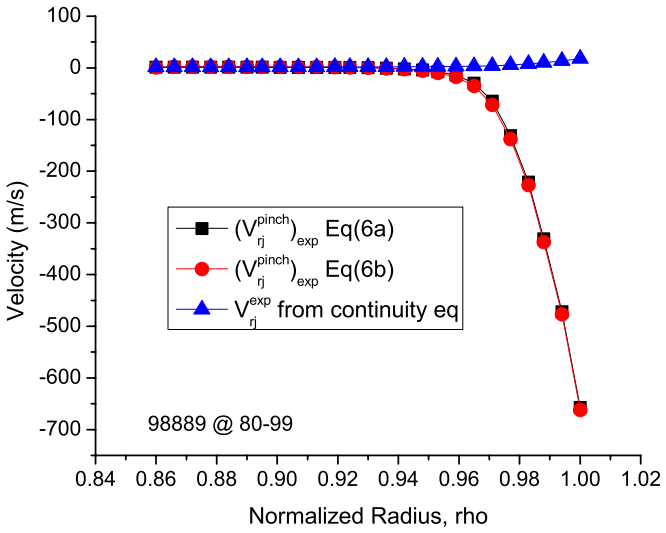

FIG. 5. (Color online) Radial pinch and particle velocities.

other processes, ν_{dj}, is larger than the interspecies collisional momentum exchange rate in the edge pedestal. The charge-exchange momentum transfer rate for deuterium was calculated and is orders of magnitude smaller than the inferred momentum transfer rate.

The experimental radial electric field is shown in Fig. 4. This quantity is determined from Eq. (4) using the measured carbon rotation velocities and pressure profile.

The deuterium poloidal rotation velocity was calculated from poloidal momentum balance[15]

$$\left(\frac{q\upsilon_{thj}f_j}{R}+\nu_{jk}+\nu_{\text{atom }j}\right)V_{\theta j}-\nu_{jk}V_{\theta k}$$
$$=-\frac{e_jV_{rj}B_\phi}{m_j}+\frac{\upsilon_{thj}f_jq}{R}\left(\frac{B_\phi K^jT_jL_{Tj}^{-1}}{e_jB^2}+\frac{\upsilon_{thj}E_r}{B_\theta}\right) \quad (14)$$

using the experimental carbon rotation velocity for $V_{\theta k}$. Here K^j is a ratio of Hirshman–Sigmar coefficients defined in Ref. 15, $\eta_{0j}=n_jm_j\upsilon_{thj}qRf_j(\nu_{jj}^*)$, with $f_j=\varepsilon^{-3/2}\nu_{jj}^*/[(1+\varepsilon^{-3/2}\nu_{jj}^*)(1+\nu_{jj}^*)]$ being an interpolation formula connecting the collisional result $f_j=1/\nu_{jj}^*$ to the strongly rotating banana and plateau regime results, and with $\nu_{jj}^*=\nu_{jj}qR/\upsilon_{thj}$.

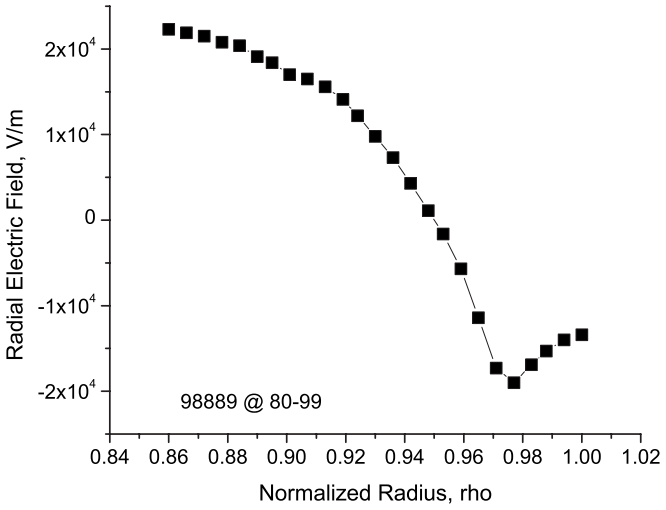

FIG. 4. Experimental radial electric fields.

IV. PINCH VELOCITY AND DENSITY PROFILE

The radial pinch velocities calculated from Eqs. (6), using experimental and calculated rotation velocities and electric field, and the experimental radial particle velocity, determined from solving the continuity equation using the neutral beam and recycling sources, are shown in Fig. 5. The recycling neutral flux was calculated with the GTEDGE integrated modeling code[16] using a 2D neutral transport calculation coupled to a two-point divertor model and a core particle and power balance benchmarked against experimental measurements of line average density, average temperature, temperature and density at the separatrix, etc.

Only the carbon rotation velocities are measured. The deuterium toroidal rotation velocity can be calculated as discussed above. Numerical evaluation using the parameters of this DIII-D shot indicates that the difference in deuterium and carbon toroidal rotation velocities given by Eq. (12) is in fact small compared to the measured carbon toroidal rotation velocity, confirming the validity of the perturbation analysis approach.

Determination of the deuterium poloidal rotation velocity is more uncertain. Calculations using different theoretical models[15] yield values that are significantly different from each other and significantly different from the measured carbon poloidal rotation velocities. We use the momentum balance calculation of poloidal velocity given by Eq. (14) to relate the poloidal deuterium rotation velocity to the measured poloidal carbon rotation velocity, but recognize that this model does not take into account viscously driven torques[17] in the edge plasma due to scrape-off layer (SOL) flows nor other poorly understood phenomena thought to affect rotation in the plasma edge.

The pinch velocities evaluated from Eq. (6) are determined primarily by the radial electric field and rotation velocity terms, with the beam momentum input and the induced toroidal electric field having a much smaller effect.

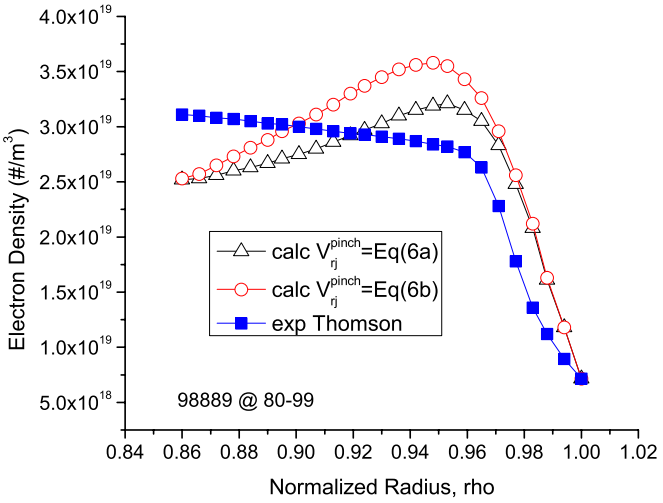

FIG. 6. (Color online) Comparison of measured and calculated electron density profiles.

With reference to Eq. (8), it is clear that the effect of the rotation velocities and electric field, acting through V_{rj}^{pinch}, is much larger than the effect of neutral recycling, acting through V_{rj}, in determining the density profile.

The electron density profiles calculated by integrating Eq. (8) and using the data shown in these figures are shown in Fig. 6. Relatively small differences in V_{rj}^{pinch} result in significant differences in the calculated density profile. Also shown is the experimental electron density profile measured with Thomson scattering. The calculated density profile exhibits a pedestal structure with about the same height and width as found with the Thomson scattering measurements. The differences in the detail shape of the calculated and Thomson density profiles are attributed to the uncertainty (discussed above) in the calculated deuterium poloidal rotation profile used to evaluate the pinch velocity from Eq. (6).

These results confirm earlier results,[9] but now use improved methods for processing the experimental data,[13,14] more systematic models for interpreting the radial angular momentum transport frequency from measured rotation velocities,[13] an improved theoretical model for the calculation of the deuterium poloidal velocity,[17] and a more accurate numerical integration of Eq. (8) to calculate the density profile. Nevertheless, uncertainties remain both in the analysis and in the input data employed.

The ability to calculate the recycling neutral ionization source that is used in the continuity equation to determine the physical radial deuterium flux V_{rj} is always questionable, primarily because of the uncertainty in determining the recycling neutral source. We model the neutral transport in two dimensions and normalize the calculated recycling source at the divertor plate to yield the measured line average density, but we do not treat the poloidal asymmetry in recycling neutral source[18] in detail. However, as indicated by Fig. 5, the uncertainties in the determination of the actual particle flux V_{rj} are not as important as the uncertainties in determining the pinch velocity V_{rj}^{pinch}.

For the parameters of this shot, the largest contribution to V_{rj}^{pinch} is the deuterium poloidal rotation velocity, which must be calculated as described above. This model does not take into account any viscous torque transfer from the SOL into the plasma edge that may be present.[17] Taking the difference in the measured carbon poloidal rotation velocity and the calculated deuterium poloidal rotation velocity as a crude measure of the uncertainty in the latter would lead to an estimate of uncertainties larger than the differences in the calculated and measured electron density profiles in Fig. 6.

V. SUMMARY AND CONCLUSIONS

Momentum and particle balance have been used to calculate the density profile in the edge pedestal, utilizing measured temperatures, rotation velocities, and electric fields, and taking into account the effect of recycling neutrals. A perturbation analysis, based on the difference in carbon and deuterium toroidal velocities being small compared to the measured carbon toroidal velocity, is employed. The effect of the rotation velocities and the radial electric field dominates the effect of the recycling neutral ionization in the calculation of the edge density profile, which was in agreement with the experimental density profile measured by Thomson scattering.

ACKNOWLEDGMENTS

The author is grateful to R. J. Groeber of General Atomics for providing the fits to the DIII-D data used in this paper and for his collaboration on several previous papers in which some of the data interpretation ideas used in this paper were first developed. This work was supported by the U.S. Department of Energy Grant No. DE-FG02-00-ER54538 with the Georgia Tech Research Corporation.

[1] A. E. Hubbard, Plasma Phys. Controlled Fusion **42**, A15 (2000).
[2] M. Kotschenreuther, W. Dorland, and Q. P. Liu, *Proceedings of the 16th Conference Plasma Physics Controlled Fusion Research*, Montreal, 1996 (IAEA, Vienna, 1997), Vol. 2, p. 371.
[3] J. E. Kinsey, R. E. Waltz, and D. P. Schissel, Proceedings of the 24th EPS Conference, Berchtesgarten, 1997, Vol. III, p. 1081.
[4] P. B. Snyder, H. R. Wilson, J. R. Ferron, L. L. Lao, A. W. Leonard, T. H. Osborne, A. D. Turnbull, D. Mossessian, M. Murikami, and X. Q. Xu, Phys. Plasmas **9**, 2037 (2002).
[5] R. L. Boivin, J. A. Getz, A. E. Hubbard, J. W. Hughes, I. H. Hutchinson, J. H. Irby, B. LaBombard, E. S. Marmar, D. Mossessian, C. S. Pitcher, J. L. Terry, B. A. Carreras, and L. W. Owen, Phys. Plasmas **7**, 1919 (2000).
[6] R. J. Groebner, M. A. Mahdavi, A. W. Leonard, T. H. Osborn, G. D. Porter, R. J. Colchin, and L. W. Owen, Phys. Plasmas **9**, 2134 (2002).
[7] M. A. Mahdavi, R. Maingi, R. J. Groebner, A. W. Leonard, T. H. Osborne, and G. Porter, Phys. Plasmas **10**, 3984 (2003).
[8] R. J. Groebner, M. A. Mahdavi, A. W. Leonard, T. H. Osborne, N. S. Wolf, G. D. Porter, P. C. Stangeby, N. S. Brooks, R. J. Colchin, and L. W. Owen, Nucl. Fusion **44**, 204 (2004).
[9] W. M. Stacey and R. J. Groebner, Phys. Plasmas **12**, 042504 (2005).
[10] J. Luxon, Nucl. Fusion **42**, 614 (2002).
[11] W. M. Stacey, Contrib. Plasma Phys. **48**, 94 (2008).
[12] J. D. Callen, R. J. Groebner, T. H. Osborne, J. M. Canik, L. W. Owen, A. Y. Pankin, T. Rafiq, T. D. Rognlien, and W. M. Stacey, "Analysis of pedestal transport," Nucl. Fusion (to be published).
[13] W. M. Stacey and R. J. Groebner, Phys. Plasmas **16**, 102504 (2009).
[14] W. M. Stacey and R. J. Groebner, Phys. Plasmas **15**, 012503 (2008).
[15] W. M. Stacey, Phys. Plasmas **15**, 012501 (2008).
[16] W. M. Stacey, Phys. Plasmas **5**, 1015 (1998); **8**, 3673 (2001); Nucl. Fusion **40**, 965 (2000).
[17] W. M. Stacey, Phys. Plasmas **16**, 062505 (2009).
[18] Z. W. Friis, W. M. Stacey, A. W. Leonard, and M. Rensink, Phys. Plasmas **17**, 022507 (2010).